Applied Mathematical Modelling 35 (2011) 285–302

Contents lists available at ScienceDirect

Applied Mathematical Modelling

journal homepage: www.elsevier.com/locate/apm

Developing new approaches for the path tubes method

Nélio Henderson [a,*], Marcelo Sampaio [b], Luciana Pena [c]

[a] Thermodynamics and Optimization Group (TOG), Instituto Politécnico, Universidade do Estado do Rio de Janeiro, 28601-970 Nova Friburgo, RJ, Brazil
[b] Eletronuclear – Eletrobrás Termonuclear S.A, 23948-00 Angra dos Reis, RJ, Brazil
[c] Laboratório de Ciências Matemáticas, Universidade Estadual do Norte Fluminense, 28013-602 Campos dos Goytacazes, RJ, Brazil

ARTICLE INFO

Article history:
Received 29 April 2008
Received in revised form 23 May 2010
Accepted 4 June 2010
Available online 10 June 2010

Keywords:
Advection equations
Path tubes method
Semi-Lagrangian algorithm

ABSTRACT

The path tubes (PT) method for advection equations is a semi-Lagrangian algorithm recently introduced in the literature. PT method is simple, physically intuitive, backward-in-time and mass-conserving algorithm, whose formulation is based on the fundaments of the mechanics of continuous media, in the light of Lagrangian methodology. In present work, we describe new approaches for PT methodology, including an absolutely accurate semi-Lagrangian scheme for 1D problems and a new and attractive discretization for multidimensional problems. In addition, we show that PT method is unconditionally stable.

1. Introduction

The advection equation can be written as follows:

$$\frac{\partial C}{\partial t} + \nabla \cdot (C\mathbf{v}) = 0. \tag{1}$$

Here, $C = C(\mathbf{x}, t)$ is a scalar function that represents the concentration of a given substance, $\mathbf{v} = \mathbf{v}(\mathbf{x}, t)$ is a specified velocity field, $\mathbf{x}$ is the spatial variable and t is the time.

Since the advection equations govern the evolution of a variety of physical phenomena, Eq. (1) is of great practical importance in the science and engineering. The velocity field can be an intricate function of the space and time, and the solution cannot be analytically calculated.

Therefore, in situations of practical interest, numerical approximations to the advection equation are necessary for solving real problems. However, it is well recognized that some methods can produce numerical diffusion, oscillatory behavior and physically unrealistic concentrations, and/or are subject to the Courant–Friedrichs–Lewy (CFL) condition, which imposes restrictions in the time step, see [1–3].

In order to overcome these problems, in a recent article we introduce the path tubes (PT) method, a simple, physically intuitive, backward-in-time, semi-Lagrangian and mass-conserving algorithm, [4].

Since the 1950s, a variety of articles have appeared in the literature, which address aspects of semi-Lagrangian algorithms in different fields of science and technology. Hence, the present method has a special relation with works of several other authors, among them we can mention, for example, Wiin-Nielsen [5], Trulio [6], Hirt et al. [7], Robert [8], Staniforth and Côté [9], Smolarkiewicz and Pudykiewicz [10], Williamson and Olson [11], Gravel and Staniforth [12] and Chilakapati [13].

In present work, we describe and analyze new approaches for PT method. In fact: (i) for the first time, we develop a 1D integral formulation for PT method which uses the Leibnitz formula, (ii) from the three-point Gauss quadrature rule, we

* Corresponding author. Fax: +55 22 25288536.
E-mail address: nelio@iprj.uerj.br (N. Henderson).

0307-904X/$ - see front matter © 2010 Elsevier Inc. All rights reserved.
doi:10.1016/j.apm.2010.06.004

present an absolutely accurate semi-Lagrangian scheme for 1D advection equations, (iii) we show that this 1D scheme is unconditionally stable, and (iv) using the change of variable formula and the trapezoidal rule, we deduct a new and attractive multidimensional discretization.

Moreover, a variety of numerical results with classical (and extremely difficult) 1D and 2D examples are shown to illustrate the robustness of the new formulations.

2. Basic principles of continuum mechanics

The path tubes method is based on the fundaments of the mechanics of continuous media in the light of Lagrangian methodology. In view of this, we introduce some physical concepts of interest related with the basic kinematics [14,15].

In continuum mechanics, a material body is characterized by the possibility of occupying different regions of the Euclidean space at different times. Given $t \in \mathbb{R}$, a three-dimensional body, for example, is idealized as a connected set in $\mathbb{R}^3$, called the configuration of the body at time t. Thus, in different instants t and $\tilde{t}$, the same body Ω is represented by two possibly different configurations Ω_t and $\Omega_{\tilde{t}}$. During the motion of the body, the location in space is given by a vector

$$\mathbf{x} = \mathbf{x}(\zeta, t), \tag{2}$$

where ζ denotes the position of an arbitrary material point ζ of Ω in the configuration related with the instant t, see Fig. 1.

The spacetime is identified with the Cartesian product $\mathbb{R}^3 \times \mathbb{R}$ of the Euclidean space $\mathbb{R}^3$ and the time axis $\mathbb{R}$. The curve in spacetime along which an arbitrary material particle ζ travels is referred to as the path line for the particle ζ. Thus, the path line of ζ is determined by following set

$$\Im_\zeta = \{(\mathbf{x}, t) \in \mathbb{R}^3 \times \mathbb{R};\ \mathbf{x} = \mathbf{x}(\zeta, t) \in \Omega_t, \quad t \in \mathbb{R}\}. \tag{3}$$

The parametric equations of a particle path are the solutions of the system of differential equations

$$\frac{d\mathbf{x}}{dt} = \mathbf{v}. \tag{4}$$

The required additional condition to solve Eq. (4) may be obtained by choosing a reference configuration, a configuration that the material particle assumed at some particular time $\tilde{t}$,

$$\mathbf{x}(\zeta, \tilde{t}) = \tilde{\mathbf{x}}. \tag{5}$$

A path tube Σ is a region in spacetime formed by union of path lines relative to all particles ζ of the given material body Ω, i.e.,

$$\Sigma = \bigcup_{\zeta \in \Omega} \Im_\zeta. \tag{6}$$

3. PT formulation in 1D

3.1. 1D Lagrangian formulation

In 1D, the position of ζ will be denoted by

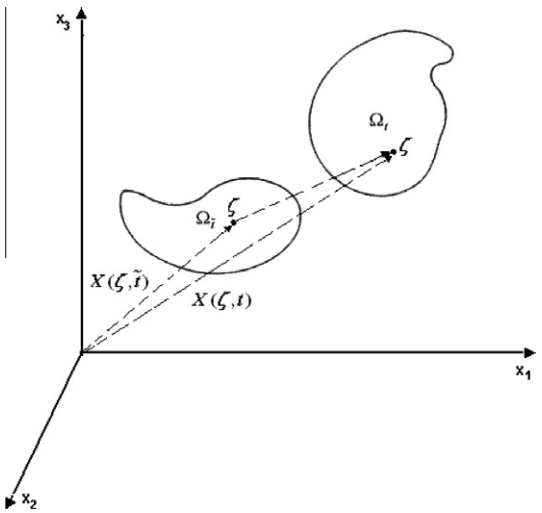

Fig. 1. Positions of an arbitrary material point ζ.

$$x = x(\zeta, t), \tag{7}$$

and the path line of ζ is determined as following

$$\Im_\zeta = \{(x,t) \in \mathbb{R} \times \mathbb{R}; \quad x = x(\zeta,t) \in \Omega_t, \quad t \in \mathbb{R}\}, \tag{8}$$

where the material body takes the particular form $\Omega_t = [x_1(t), x_2(t)]$. In this case, the parametric equations of a particle path are the solutions of the differential equation

$$\frac{dx}{dt} = v, \tag{9}$$

where $v = v(x,t)$ is a specified velocity field in 1D. The required additional condition to solve Eq. (9) is given by

$$x(\tilde{t}) = \tilde{x}. \tag{10}$$

The 1D advection equation can be written as follows,

$$\frac{\partial C}{\partial t} + \frac{\partial}{\partial x}(Cv) = 0. \tag{11}$$

Integrating Eq. (11) along the path tube

$$\Sigma = \bigcup_{\zeta \in \Omega} \{(x,\tilde{t}) \in \mathbb{R} \times \mathbb{R}; \quad x = x(\zeta,\tilde{t}) \in \Omega_{\tilde{t}} = [x_1(\tilde{t}),\ x_2(\tilde{t})],\ t \leqslant \tilde{t} \leqslant t + \Delta t\}, \tag{12}$$

which is defined in the interval $[t, t+\Delta t]$,we obtain

$$\int_t^{t+\Delta t} \int_{x_1(t)}^{x_2(t)} \left[\frac{\partial C}{\partial t} + \frac{\partial (vC)}{\partial x}\right] dx dt = 0, \tag{13}$$

Eq. (13) can be written as

$$\int_t^{t+\Delta t} \left[\int_{x_1(t)}^{x_2(t)} \frac{\partial C}{\partial t} dx + [v(x_2(t),t)C(x_2(t),t) - v(x_1(t),t)C(x_1(t),t)]\right] dt = 0. \tag{14}$$

On the other hand, by Leibnitz formula (see [16]) we have

$$\int_{x_1(t)}^{x_2(t)} \frac{\partial C}{\partial t} dx + \left[\frac{dx_2(t)}{dt} C(x_2(t),t) - \frac{dx_1(t)}{dt} C(x_1(t),t)\right] = \frac{d}{dt} \int_{x_1(t)}^{x_2(t)} C(x,t) dx. \tag{15}$$

Using Eq. (9), the relation in Eq. (15) becomes

$$\int_{x_1(t)}^{x_2(t)} \frac{\partial C}{\partial t} dx + [v(x_2(t),t)C(x_2(t),t) - v(x_1(t),t)C(x_1(t),t)] = \frac{d}{dt} \int_{x_1(t)}^{x_2(t)} C(x,t) dx. \tag{16}$$

From Eqs. (14) and (16), we obtain

$$\int_t^{t+\Delta t} \left[\frac{d}{dt} \int_{x_1(t)}^{x_2(t)} C(x,t) dx\right] dt = 0. \tag{17}$$

Thus, by the fundamental theorem of calculus, Eq. (17) can be written as

$$\int_{x_1(t+\Delta t)}^{x_2(t+\Delta t)} C(x, t+\Delta t) dx = \int_{x_1(t)}^{x_2(t)} C(x,t) dx. \tag{18}$$

This 1D Lagrangian formulation (Eq. (18)) shows that the mass is conserved along the path tube.

3.2. 1D discretization scheme

In order to obtain a discretization scheme, in any instant, we use uniform cell centered grids, as shown in Fig. 2. The interval $I_j = [x_{j-1/2}, x_{j+1/2}]$ represents an arbitrary grid cell, whose length is $\Delta x = x_{j+1/2} - x_{j-1/2}$, for all j.

In a backtracking step, we solve ordinary differential equations, as indicated in Eq. (9), subject to final condition $x(t+\Delta t) = \tilde{x}$. In agreement with the illustration in Fg. 3, using backtracking of the path lines, we obtain the interval $[x_-, x_+]$, the image of the cell $I_j = [x_{j-1/2}, x_{j+1/2}]$ in the instant t. Thus, it follows that the points x_- and x_+ denote the solutions obtained by solving the ordinary differential equation $dx/dt = v$, with final conditions $\tilde{x} = x_{i-1/2}$ and $\tilde{x} = x_{i+1/2}$, respectively.

Hence, we can write the 1D Lagrangian formulation (Eq. (18)) for each path tube obtained by discretization, as shown in Fig. 3. Thus, for all j, we have

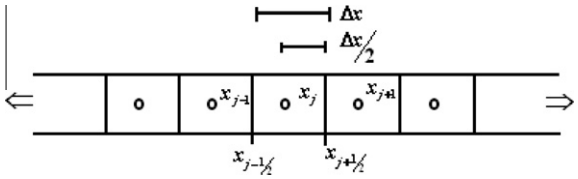

Fig. 2. The 1D grid.

$$\int_{x_{j-1/2}}^{x_{j+1/2}} C(x,t+\Delta t)dx = \int_{x_-}^{x_+} C(x,t)dx. \tag{19}$$

In each instant $t + \Delta t$, consider

$$C_j^{(n+1)} \equiv \frac{1}{\Delta x}\int_{x_{j-1/2}}^{x_{j+1/2}} C(x,t+\Delta t)dx, \tag{20}$$

the average value of the concentration on the jth cell $I_j = [x_{j-1/2}, x_{j+1/2}]$.

From Eqs. (19) and (20), we obtain the explicit scheme

$$C_j^{(n+1)} = \frac{1}{\Delta x}\int_{x_-}^{x_+} C(x,t)dx. \tag{21}$$

This 1D scheme (Eq. (21)) is a numerical adaptation of the Lagrangian formulation summarized initially in Eq. (18), being (locally) a mass-conserving algorithm.

In order to calculate C in the time level $(n + 1)$, the schemes in Eq. (21) demands the calculation of integrals $\int_{x_-}^{x_+} C(x,t)dx$. In the present work, these integrals are approximated by the three-point Gauss quadrature rule, see, for example [17,18]. Thus, we obtain

$$\int_{x_-}^{x_+} C(x,t)dx \cong \frac{(x_+ - x_-)}{18}[5(C_a + C_b) + 8C_c]. \tag{22}$$

In Eq. (22), we have $C_a \equiv C(x_a,t)$, $C_b \equiv C(x_b,t)$ and $C_c \equiv C(x_c,t)$; where

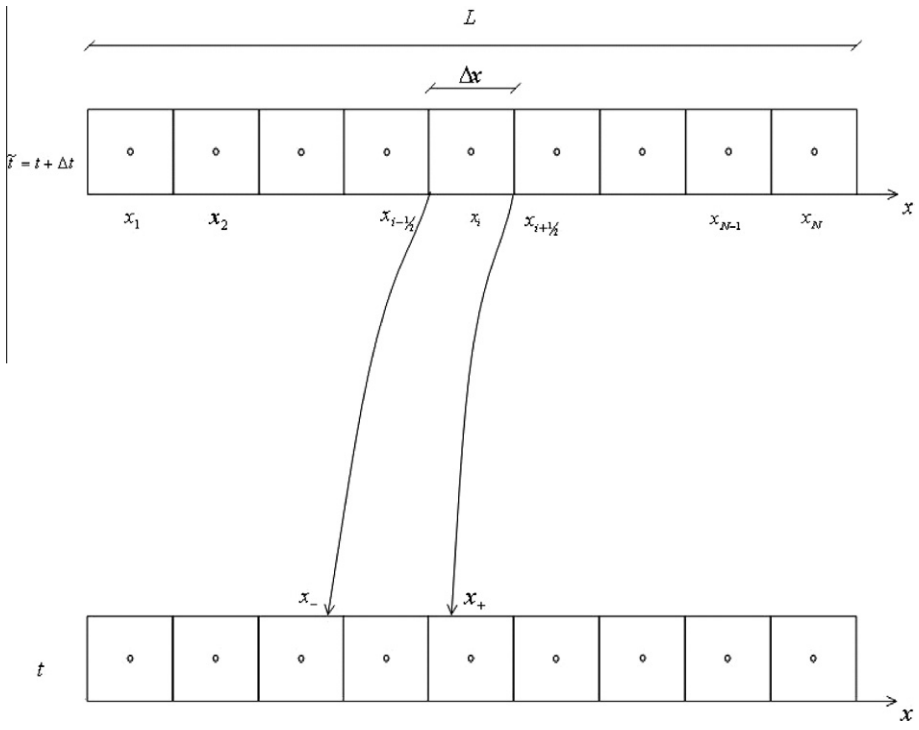

Fig. 3. A path tube in $\mathbb{R} \times \mathbb{R}$.

$$x_a = (x_+ + x_-)/2 - [(x_+ - x_-)/2]\sqrt{3/5}, \tag{23}$$

$$x_b = (x_+ + x_-)/2 - [(x_+ + x_-)/2]\sqrt{3/5}, \tag{24}$$

$$x_c = (x_+ + x_-)/2. \tag{25}$$

In each instant t, the only known values are $C_j^{(n)}$, for all j, i.e., the values of C in the center of the cells. Using these concentrations, C_a,C_b and C_c are calculated in the following way: if, in instant t,$I_q = [x_{q-1/2},x_{q+1/2}]$ denotes the cell that contains x_a, then C_a is approximated by cubic Lagrange interpolation of the values of the concentration in I_q and in the neighbour cells, I_{q-1}, I_{q+1} and I_{q+2} (or I_{q-2}). The values C_b and C_c are calculated in similar form. In order to avoid oscillatory behavior, our computational experience shows that this procedure requires a small adjustment. The result of the interpolation cannot exceed the concentration values in the interpolation cells. Thus, when necessary, we replaced the calculated value by the maximum value of the concentration in the interpolation cells. A similar fact happens with the minimum of C in the interpolation cells. Thus, we used the following limiter: if $x_a \in I_q = [x_{q-1/2},x_{q+1/2}]$, then $C(x_a,t) = C_a$ is approximated by relations

$$C_a \cong \begin{cases} m, & \text{if } P_3(x_a) < m \\ P_3(x_a), & \text{if } m \leqslant P_3(x_a) \leqslant M \\ M, & \text{if } P_3(x_a) > M \end{cases} \tag{26}$$

where

$$P_3(x) = \sum_{i=q-1}^{q+2} C_i^{(n)} \prod_{\substack{k=q-1 \\ k\neq i}}^{q+2} \frac{x - x_k}{x_i - x_k} \tag{27}$$

is the interpolation polynomial, and the values m and M are given by

$$m = \text{Min } \{C_{q-1}^{(n)}, C_q^{(n)}, C_{q+1}^{(n)}, C_{q+2}^{(n)}\}, \tag{28}$$

$$M = \text{Max } \{C_{q-1}^{(n)}, C_q^{(n)}, C_{q+1}^{(n)}, C_{q+2}^{(n)}\}. \tag{29}$$

In boundary-initial-value problems, if I_q is a boundary cell, the boundary condition value is included in this modified cubic Lagrange interpolation. This naturally incorporates the boundary conditions, when they exist.

If $m \leqslant P_3(x_a) \leqslant M$, then an error $E(x_a) \equiv C_a - P_3(x_a)$ occur in the approximation $C_a \cong P_3(x_a)$. This interpolation error can be estimated as follows.

Proposition 1. *Assume that each of the partial derivatives $\partial^k C(x,t)/\partial x^k, 1 \leqslant k \leqslant 5$, exists and is continuous in $[x_{q-1},x_{q+2}]$. Then for all point $x_a \in I_q = [x_{q-1/2},x_{q+1/2}]$ there exists a number $\xi_a \in [x_{q-1},x_{q+2}]$ such that*

$$|E(x_a)| \leqslant \frac{3(\Delta x)^4}{64}\left|\frac{\partial^5 C(\xi_a,t)}{\partial x^5}\right|. \tag{30}$$

Proof. Let $\omega(x) = (x_{q-1} - x)(x_q - x)(x_{q+1} - x)(x_{q+2} - x)$. It is well-known that, in these conditions, see [18], there exists $\xi_a \in [x_{q-1},x_{q+2}]$ satisfying

$$E(x_a) \equiv C_a - P_3(x_a) = \frac{\omega(x_a)}{120}\frac{\partial^5 C(\xi_a,t)}{\partial x^5}. \tag{31}$$

Since

$$|\omega(x_a)| \leqslant \frac{45}{8}(\Delta x)^4, \tag{32}$$

then, from Eqs. (31) and (32), follows the estimate in Eq. (30).

As we can see, Eq. (30) shows that $|E(x_a)| \to 0$, whenever $\Delta x \to 0$. □

4. Stability analysis

In the present work, the stability analysis for PT method is performed in 1D, in agreement with the scheme shown in Eq. (21).

To proceed with the stability analysis, we consider a sufficiently fine grid, such that the scheme in Eq. (21) can be approximated by

$$C_j^{(n+1)} \cong \frac{1}{\Delta x} C(\hat{x},t)\int_{x_-}^{x_+} dx, \tag{33}$$

where $\hat{x}$ is a point in $[x_-,x_+]$ obtained by backtracking of the center of $I_j = [x_{j-1/2},x_{j+1/2}]$.

We also suppose that the flow is incompressible. In this case, the cell $I_j = [x_{j-1/2},x_{j+1/2}]$ is not deformed by backtracking. Thus,

$$\int_{x_-}^{x_+} dx = \int_{x_{j-1/2}}^{x_{j+1/2}} dx = \Delta x. \tag{34}$$

From Eqs. (33) and (34), we can write

$$C_j^{(n+1)} = C(\hat{x}, t). \tag{35}$$

Since the flow is incompressible, then $\partial v/\partial x = 0$, i.e., v = constant. In the present wok, we will assume $v > 0$. Therefore, by backtracking, we have

$$\int_{x_j}^{\hat{x}} dx = v \int_{t+\Delta t}^{t} dt \tag{36}$$

or

$$\hat{x} = x_j - v\Delta t. \tag{37}$$

From Eq. (37), we can affirm that there exists an index $p \geqslant 0$ such that

$$x_{j-p-1} \leqslant \hat{x} \leqslant x_{j-p}, \tag{38}$$

where x_{j-p} is the center of the cell $I_{j-p} = [x_{j-p-1/2},x_{j-p+1/2}]$. In other words

$$\hat{x} = [j-p]\Delta x - \alpha\Delta x, \text{ for some } \alpha \in [0,1]. \tag{39}$$

Thus, we obtain the scheme

$$C_j^{(n+1)} = C^{(n)}([j-p]\Delta x - \alpha\Delta x). \tag{40}$$

Since we can have $\alpha \neq 0$ and $\alpha \neq 1$, then we need an interpolation process. Considering the cubic Lagrange interpolation, we can write

$$C_j^{(n+1)} = C^{(n)}([j-p]\Delta x - \alpha\Delta x) = \sum_{k=j-p-1}^{j-p+2} C_k^{(n)} \prod_{\substack{s\neq k \\ s=j-p-1}}^{j-p+2} \frac{x - x_s}{x_k - x_s}. \tag{41}$$

After some algebraic effort, we can show that

$$C^{(n)}([j-p]\Delta x - \alpha\Delta x) = \sum_{k=j-p-1}^{j-p+2} C_k^{(n)} \prod_{\substack{s\neq k \\ s=j-p-1}}^{j-p+2} \frac{x - x_s}{x_k - x_s} = \eta_1 C_{j-p-1}^{(n)} + \eta_2 C_{j-p}^{(n)} + \eta_3 C_{j-p+1}^{(n)} + \eta_4 C_{j-p+2}^{(n)}, \tag{42}$$

i.e.,

$$C_j^{(n+1)} = \eta_1 C_{j-p-1}^{(n)} + \eta_2 C_{j-p}^{(n)} + \eta_3 C_{j-p+1}^{(n)} + \eta_4 C_{j-p+2}^{(n)}, \tag{43}$$

where

$$\eta_1 = \frac{\alpha(\alpha+1)(\alpha+2)}{6}, \tag{44}$$

$$\eta_2 = \frac{(1-\alpha)(\alpha+1)(\alpha+2)}{2}, \tag{45}$$

$$\eta_3 = \frac{\alpha(\alpha-1)(\alpha+2)}{2}, \tag{46}$$

$$\eta_4 = \frac{\alpha(1-\alpha)(\alpha+1)}{6}. \tag{47}$$

To study the stability of the scheme in Eq. (43), we consider von Neumann's method, see [2], for example. Thus, we need investigate a propagation of the term

$$C_k^{(n)} = \xi^n e^{ik\beta\Delta x}, \tag{48}$$

where $i = \sqrt{-1}$, β is the wave number and ξ is the amplification factor. We can write Eq. (48) in the form

$$C_k^{(n)} = \xi^n e^{ik\phi}. \tag{49}$$

where $\phi = \beta\Delta x$ is the phase angle.

Substitution of $C_k^{(n)}$, as defined in Eq. (49), onto both sides of Eq. (43) shows that

$$\xi = e^{-ip\phi}(\eta_1 e^{-i\phi} + \eta_2 + \eta_3 e^{i\phi} + \eta_4 e^{i2\phi}). \tag{50}$$

Eq. (50) can be written in the equivalent form,

$$\xi = e^{-ip\phi}(A + iB), \tag{51}$$

where

$$A = (\eta_1 + \eta_3)\cos\phi + \eta_4 \cos 2\phi + \eta_2, \tag{52}$$
$$B = (\eta_3 - \eta_1)\sin\phi + \eta_4 \sin 2\phi. \tag{53}$$

It is not difficult to show the identity

$$A^2 + B^2 = (\eta_1^2 + \eta_2^2 + \eta_3^2 + \eta_4^2) + 2\eta_1\eta_3\cos^2\phi - 2\eta_1\eta_3\sin^2\phi + 2[\eta_3\eta_4 + \eta_2(\eta_1 + \eta_3)]\cos\phi + 2\eta_2\eta_4\cos 2\phi + 2\eta_1\eta_4\cos 3\phi. \tag{54}$$

Thus,

$$A^2 + B^2 \leqslant (\eta_1^2 + \eta_2^2 + \eta_3^2 + \eta_4^2) + 2(\eta_1\eta_2 + \eta_1\eta_3 + \eta_1\eta_4 + \eta_2\eta_3 + \eta_2\eta_4 + \eta_3\eta_4) = (\eta_1 + \eta_2 + \eta_3 + \eta_4)^2. \tag{55}$$

Therefore, we have

$$|\xi| = \sqrt{A^2 + B^2} \leqslant |(\eta_1 + \eta_2 + \eta_3 + \eta_4)|. \tag{56}$$

But, from Eqs. (44)–(47), we obtain

$$\eta_1 + \eta_2 + \eta_3 + \eta_4 = 1 - \alpha, \quad \alpha \in [0, 1]. \tag{57}$$

Thus, Eqs. (56) and (57) show that PT method satisfies the necessary and sufficient condition for stability,

$$|\xi| \leqslant 1, \text{ for all } \phi \text{ and } \alpha \in [0, 1]. \tag{58}$$

We have proved the following result.

Proposition 2. *For incompressible flows, PT method is unconditionally stable.*

5. PT formulation in multidimensions

5.1. The multidimensional Lagrangian formulation

The following proposition is the key result used in the determination of the Lagrangian formulation for PT method in multidimensions [4].

Proposition 3 (Reynolds transport theorem). *Let Ω_t be a material volume representing the configuration of a body at some instant t, which moves with velocity $\mathbf{v} = \mathbf{v}(\mathbf{x},t)$. If $\Psi = \Psi(\mathbf{x},t)$ is any continuously differentiable function of time and position, then*

$$\int_{\Omega_t}\left[\frac{\partial\Psi}{\partial t} + \nabla\cdot(\Psi\mathbf{v})\right]d\mathbf{x} = \frac{d}{dt}\int_{\Omega_t}\Psi d\mathbf{x}, \tag{59}$$

where d/dt denotes the Lagrangian derivative (or material derivative).

Proof. See [14].

Integrating the advection equation (Eq. (1)) along the multidimensional path tube

$$\Sigma = \bigcup_{\zeta\in\Omega}\{(\mathbf{x},\tilde{t}) \in \mathbb{R}^n \times \mathbb{R};\ \text{where } n = 2,3,\ \mathbf{x} = \mathbf{x}(\zeta,\tilde{t}) \in \Omega_{\tilde{t}} \subset \mathbb{R}^n \text{ and } t \leqslant \tilde{t} \leqslant t + \Delta t\}, \tag{60}$$

we obtain

$$\int_t^{t+\Delta t}\int_{\Omega_t}\left[\frac{\partial C}{\partial t} + \nabla\cdot(C\mathbf{v})\right]d\mathbf{x}dt = 0. \tag{61}$$

Eq. (61) and the Reynolds transport theorem indicate that

$$\int_t^{t+\Delta t}\left(\frac{d}{dt}\int_{\Omega_t} C d\mathbf{x}\right)dt = 0. \tag{62}$$

By definition of material derivative, see [14], we have

$$\frac{d}{dt}\int_{\Omega_t} C d\mathbf{x} = \lim_{\Delta t\to 0}\left[\frac{\int_{\Omega_{t+\Delta t}} C d\mathbf{x} - \int_{\Omega_t} C d\mathbf{x}}{\Delta t}\right]. \tag{63}$$

Then, by the fundamental theorem of calculus, we may express Eq. (62) as

$$0 = \int_t^{t+\Delta t}\left(\frac{d}{dt}\int_{\Omega_t} C d\mathbf{x}\right)dt = \int_{\Omega_{t+\Delta t}} C d\mathbf{x} - \int_{\Omega_t} C d\mathbf{x}. \tag{64}$$

Thus, we obtain the multidimensional Lagrangian formulation

$$\int_{\Omega_{t+\Delta t}} C(\mathbf{x}, t+\Delta t) d\mathbf{x} = \int_{\Omega_t} C(\mathbf{x}, t) d\mathbf{x}. \tag{65}$$

Eq. (65) shows that mass is conserved also along the multidimensional path tubes.

5.2. A new multidimensional discretization

Let $|\Omega_{t+\Delta t}| = \int_{\Omega_{t+\Delta t}} d\mathbf{x}$ be the measure of the set $\Omega_{t+\Delta t}$, and define

$$C^{(n+1)} \equiv \frac{1}{|\Omega_{t+\Delta t}|}\int_{\Omega_{t+\Delta t}} C(\mathbf{x}, t+\Delta t) d\mathbf{x} \tag{66}$$

as the average value of the concentration on $\Omega_{t+\Delta t}$. From Eqs. (65) and (66), we obtain the multidimensional explicit formula for PT method:

$$C^{(n+1)} = \frac{1}{|\Omega_{t+\Delta t}|}\int_{\Omega_t} C(\mathbf{x}, t) d\mathbf{x}. \tag{67}$$

In present section, we introduce a new discretization for Eq. (67). This new scheme for the path tubes method will be developed using the change of variable formula for multiple integrals, a multidimensional integration rule, and an interpolation technique in multidimensions.

We consider an uniform grid with blocks centered, where (on two-dimensional spaces, for example) an arbitrary block is described by $\Omega_{i,j} = [x_{i-1/2}, x_{i+1/2}] \times [y_{j-1/2}, y_{j+1/2}]$, with grid spacing $\Delta x = x_{i+1/2} - x_{i-1/2}$ and $\Delta y = y_{j+1/2} - y_{j-1/2}$, and area $|\Omega_{i,j}| = \Delta x \Delta y$, for all i and j, see Fig. 4.

Thus, according to the scheme in Eq. (67), in the level of time $n+1$ the average value of the concentration C on the block $\Omega_{i,j}$ is $C_{i,j}^{(n+1)} = \frac{1}{|\Omega_{i,j}|}\int_{D_t} C(\mathbf{x}, t) d\mathbf{x}$, i.e.,

$$C_{i,j}^{(n+1)} = \frac{1}{\Delta x \Delta y}\int_{D_t} C(x, y, t) dx dy, \tag{68}$$

where D_t represent the image set of $\Omega_{i,j}$ (at some time t) obtained by backtracking of the path lines that start on the time $t + \Delta t$.

More specifically, we can say that D_t is the image set of the block $\Omega_{i,j}$ under φ_t, where $\varphi_t : \Omega_{i,j} \subset \mathbb{R}^2 \to D_t$, given by $\varphi_t(x, y) = \left(\varphi_t^{(1)}(x, y), \varphi_t^{(2)}(x, y)\right)$, is a bijective mapping of $\Omega_{i,j}$ onto D_t, see [4]. This mapping (which determines the backtrack-

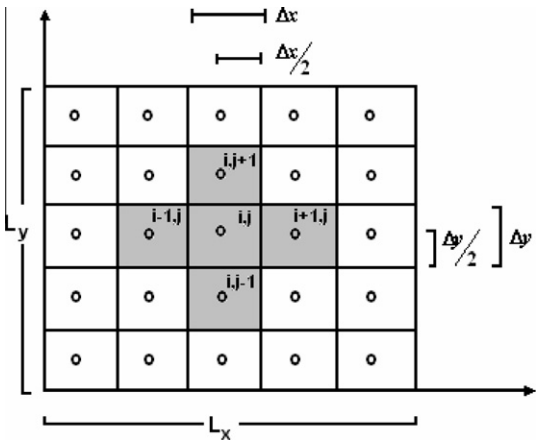

Fig. 4. The two-dimensional grid.

ing of the path lines) is obtained by solving the system of differential equations shown in Eq. (4), subject to final conditions as $x(t+\Delta t)=\tilde{x}$ and $y(t+\Delta t)=\tilde{y}$. Thus, using the change of variable formula, see [16], we can rewrite the integral in Eq. (68) as an integral over the block Ω_{ij}, i.e.,

$$C_{ij}^{(n+1)}=\frac{1}{\Delta x\Delta y}\int_{y_{i-1/2}}^{y_{i+1/2}}\int_{x_{i-1/2}}^{x_{i+1/2}}C(x,y,t)|J_t(x,y)|dxdy, \tag{69}$$

where

$$J_t(x,y)=\begin{vmatrix}\frac{\partial\varphi_t^{(1)}(x,y)}{\partial x} & \frac{\partial\varphi_t^{(1)}(x,y)}{\partial y}\\ \frac{\partial\varphi_t^{(2)}(x,y)}{\partial x} & \frac{\partial\varphi_t^{(2)}(x,y)}{\partial y}\end{vmatrix} \tag{70}$$

is the Jacobian determinant of ϕ_t.

As in Section 3.2, the integral in Eq. (69) can also be approximated by the three-point Gauss quadrature rule. Since, for multidimensional problems, this method requires many integration points, in present work we use the trapezoidal rule, see [18]. Thus, Eq. (69) becomes

$$\begin{aligned}C_{ij}^{(n+1)}=\frac{1}{4}\Big\{&|J_t(x_{i+1/2},y_{j+1/2})|C^{(n)}(\varphi_t(x_{i+1/2},y_{j+1/2}))+|J_t(x_{i-1/2},y_{j+1/2})|C^{(n)}(\varphi_t(x_{i-1/2},y_{j+1/2}))\\&+|J_t(x_{i+1/2},y_{j-1/2})|C^{(n)}(\varphi_t(x_{i+1/2},y_{j-1/2}))+|J_t(x_{i-1/2},y_{j-1/2})|C^{(n)}(\varphi_t(x_{i-1/2},y_{j-1/2}))\Big\}.\end{aligned} \tag{71}$$

In Eq. (71), the four values of $C^{(n)}$ are obtained by backtracking of the path lines that start on the four vertexes of the block $\Omega_{ij}=[x_{i-1/2},x_{i+1/2}]\times[y_{j-1/2},y_{j+1/2}]$.

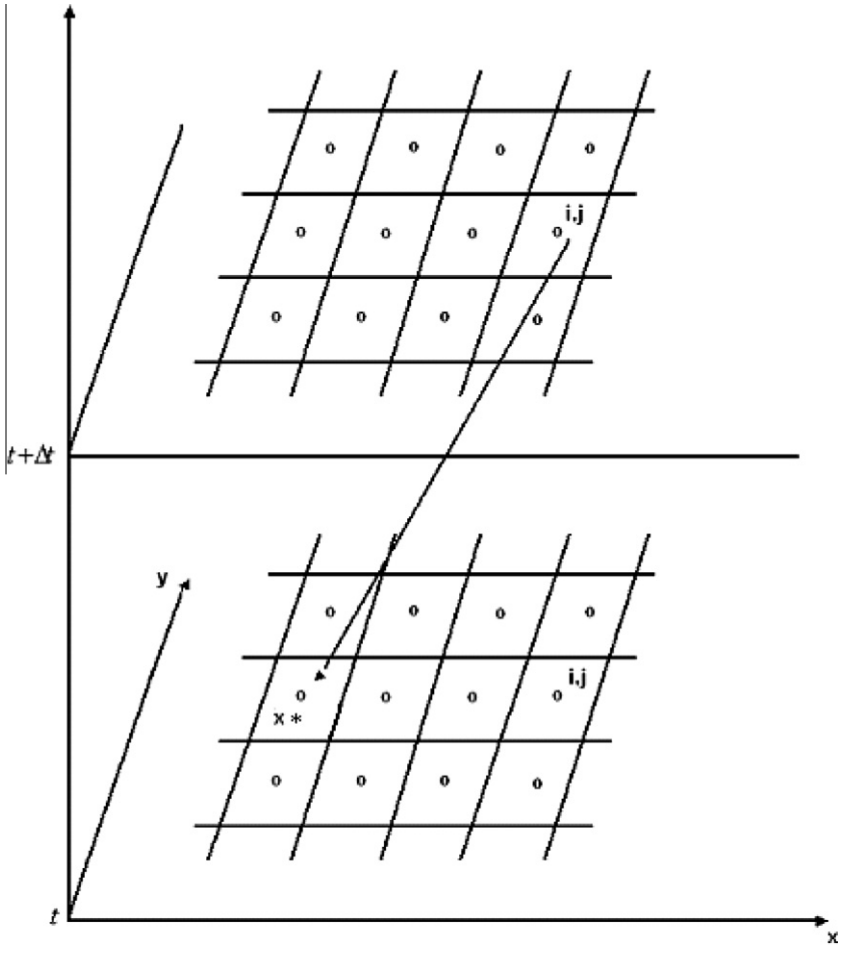

Fig. 5. A point obtained by backtracking is not necessarily the center of a block.

Here, in Eq. (71), the partial derivatives that constitute the determinants are approximate by finite differences, as shown in the examples below:

$$\frac{\partial\varphi_t(x_{i+1/2},y_{j+1/2})}{\partial x}\simeq\frac{\phi_t(x_{i+1/2}+h_x,y_{j+1/2})-\varphi_t(x_{i+1/2},y_{j+1/2})}{h_x}, \tag{72}$$

$$\frac{\partial\varphi_t(x_{i-1/2},y_{j-1/2})}{\partial y}\simeq\frac{\varphi_t(x_{i-1/2},y_{j-1/2}+h_y)-\varphi_t(x_{i-1/2},y_{j-1/2})}{h_y}. \tag{73}$$

From Eqs. (72) and (73) we can see that each of the partial derivative above requires a new backtracking step. To avoid these additional efforts, and to keep the mapping φ_t constrained to the vertexes of each block, we consider $h_x = \Delta x$ and $h_y = \Delta y$. Thus, the examples in Eqs. (72) and (73) become, respectively:

$$\frac{\partial\varphi_t(x_{i+1/2},y_{j+1/2})}{\partial x}\simeq\frac{\varphi_t(x_{i+3/2},y_{j+1/2})-\varphi_t(x_{i+1/2},y_{j+1/2})}{\Delta x}, \tag{74}$$

$$\frac{\partial\varphi_t(x_{i-1/2},y_{j-1/2})}{\partial y}\simeq\frac{\varphi_t(x_{i-1/2},y_{j+1/2})-\varphi_t(x_{i-1/2},y_{j-1/2})}{\Delta y}. \tag{75}$$

Now, we have a new numerical semi-Lagrangian explicit scheme. However, since a point obtained by backtracking is not necessarily the center of a block, see Fig. 5, we observe that this scheme is not still complete. To complete it, we consider a multidimensional numerical interpolation.

Here, we use a two-dimensional interpolation which has an entirely similar form to 1D modified cubic Lagrangian interpolation given in Eq. (26). Thus, if $(x_a,y_b)\in[x_{q-1/2},x_{q+1/2}]\times[y_{r-1/2},y_{r+1/2}]$ and $(x_a,y_b)\neq(x_q,y_r)$, then $C(x_a,y_b,t)=C_{a,b}$ is approximated by the following interpolation:

$$C_{a,b}\cong\begin{cases} m_{x,y}, & \text{if } P_3(x_a,y_b)<m_{x,y}\\ P_3(x_a,y_b), & \text{if } m_{x,y}\leqslant P_3(x_a,y_b)\leqslant M_{x,y}\\ M_{x,y}, & \text{if } P_3(x_a,y_b)>M_{x,y}\end{cases} \tag{76}$$

where

$$P_3(x,y)=\sum_{j=r-1}^{r+2}\left(\sum_{i=q-1}^{q+2}C^{(n)}(x_i,y_j)\prod_{\substack{k=q-1\\k\neq i}}^{q+2}\frac{x-x_k}{x_i-x_k}\right)\prod_{\substack{s=r-1\\s\neq j}}^{r+2}\frac{y-y_s}{y_j-y_s}, \tag{77}$$

$$m_{x,y}=\text{Min}\ \{C^{(n)}(x_i,y_j);\quad \forall i=q-1,\ldots,q+2 \text{ and } j=r-1,\ldots,r+2\}, \tag{78}$$

$$M_{x,y}=\text{Max}\ \{C^{(n)}(x_i,y_j);\quad \forall i=q-1,\ldots,q+2 \text{ and } j=r-1,\ldots,r+2\}. \tag{79}$$

6. Numerical examples in 1D

In this section, we present examples involving the 1D transport of concentration-hills by incompressible (Example 1–3) and compressible (Example 4) flows. We consider the differential equation

$$\frac{\partial C}{\partial t}+\frac{\partial(Cv)}{\partial x}=0, \tag{80}$$

with appropriate conditions.

In all the examples, we use a grid with 400 points and the path lines are evaluated analytically.

6.1. Example 1: Advancing front (with discontinuity)

In this example, we consider a boundary-initial-value problem: Eq. (80) with velocity $v = 0.5$, initial data

$$C(x,0)=0;\ x\in[0,12800] \tag{81}$$

and subject to boundary conditions

$$C(0,t)=1;\quad 0<t\leqslant t_f, \tag{82}$$

$$C(12800,t)=0;\quad 0<t\leqslant t_f. \tag{83}$$

In Fig. 6, the solutions computed by PT method are shown for several values of Δt. We see that all the numerical solutions to the above problem at $t_f = 9600$ place the jump in approximated the correct place, $x = 4800$.

An analysis of Fig. 6 indicates that our methodology is capable to describe the discontinuity, mainly if Δt is sufficiently large. We can observe that the more accurate numerical solution is reached just when $\Delta t = t_f = 9600$, where the Courant number (N_{Co}) is 300. All the time steps shown in Fig. 6 are highly prohibitive for methods subject to CFL condition, given by

$$N_{\mathrm{Co}} \equiv \frac{|v|\Delta t}{\Delta x} \leqslant 1. \tag{84}$$

6.2. Example 2: Transport of irregular signal (with discontinuity)

Here, we consider a Cauchy problem: Eq. (80) with velocity $v = 1$ and initial data

$$C(x,0) = 2 + \sigma(x)\left[1 + 0.3\sin\left(\frac{2\pi x}{9}\right)\right]\left[1 + 0.4\sin\left(\frac{2\pi x}{10}\right)\right]; \quad \forall x \in [8,39], \tag{85}$$

where

$$\sigma(x) = \begin{cases} -1, & 8 \leqslant x \leqslant 28 \\ 1, & 28 < x \leqslant 39 \end{cases}. \tag{86}$$

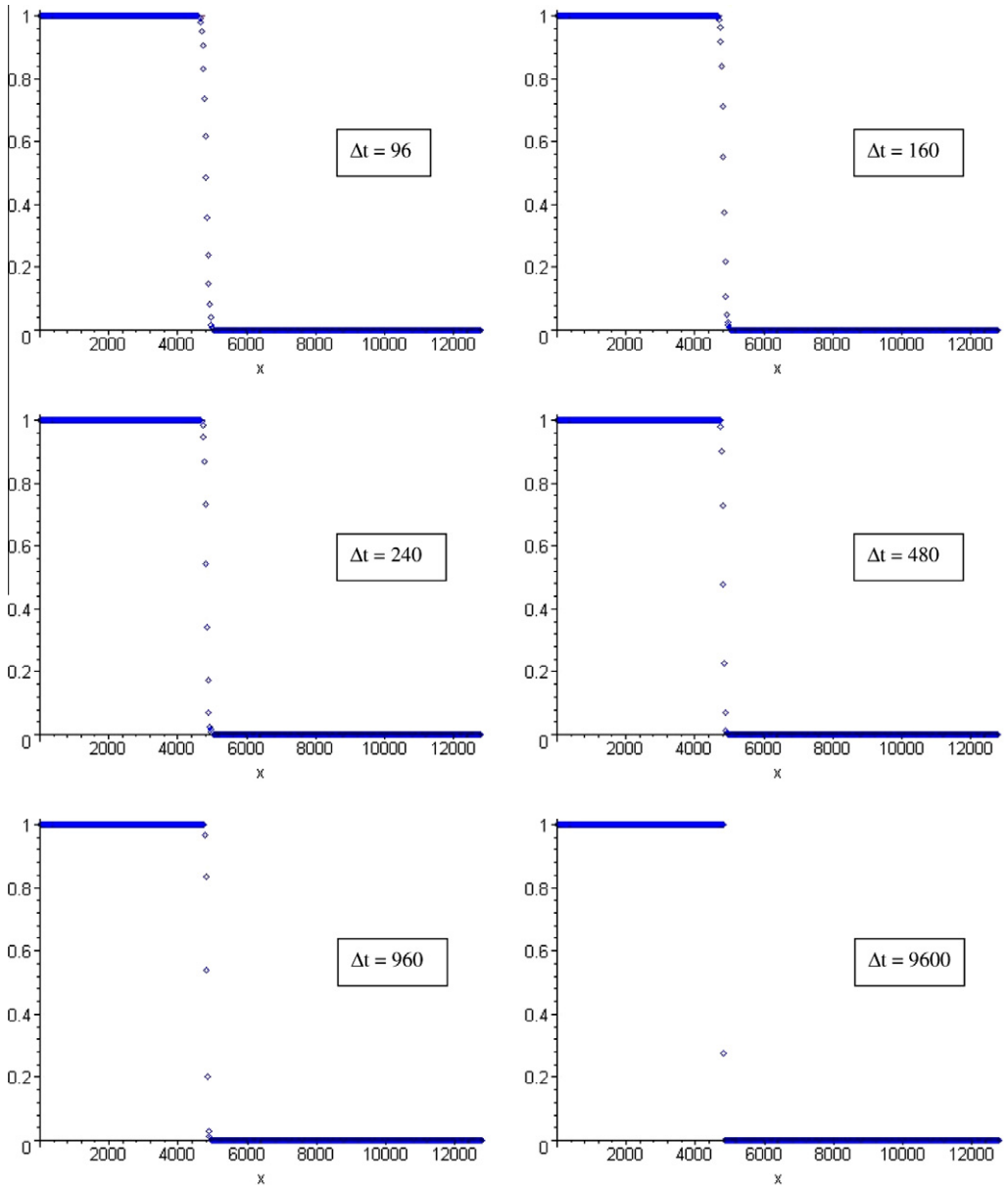

Fig. 6. Numerical solution of Example 1 at $t_f = 9600$ for different values of Δt.

In Fig. 7, the solutions computed by PT method are compared with the exact solutions, for several values of Δt. The numerical solutions are shown as curves with circles. We see that the numerical solutions at $t_f = 5$ are in agreement with the exact solutions, for several values of Δt. In this example, we observe that $N_{Co} = 1.29$, if $\Delta t = 0.1$, and $N_{Co} = 64.52$, if $\Delta t = t_f = 5$. Again, the more accurate numerical solution is reached exactly in the maximum value $\Delta t = t_f$.

6.3. Example 3: Transport of a triangular pulse

In this test, we consider Eq. (80) with velocity $v = 0.5$, $x \in [0,12800]$ and initial data

$$C(x,0) = \begin{cases} 1 - |x - x_0|; & |x - x_0| < l_0 \\ 0; & \text{otherwise} \end{cases}, \tag{87}$$

where $x_0 = 2000$ and $l_0 = 264$. Exact and numerical solutions are exhibited in Fig. 8 at $t_f = 9600$, for different values of Δt. As in Example 1, this example uses very large time steps. When $\Delta t = t_f = 9600$ (and the Courant number is 300) the numerical solution presents better agreement with the exact solution, even in the sharp corners.

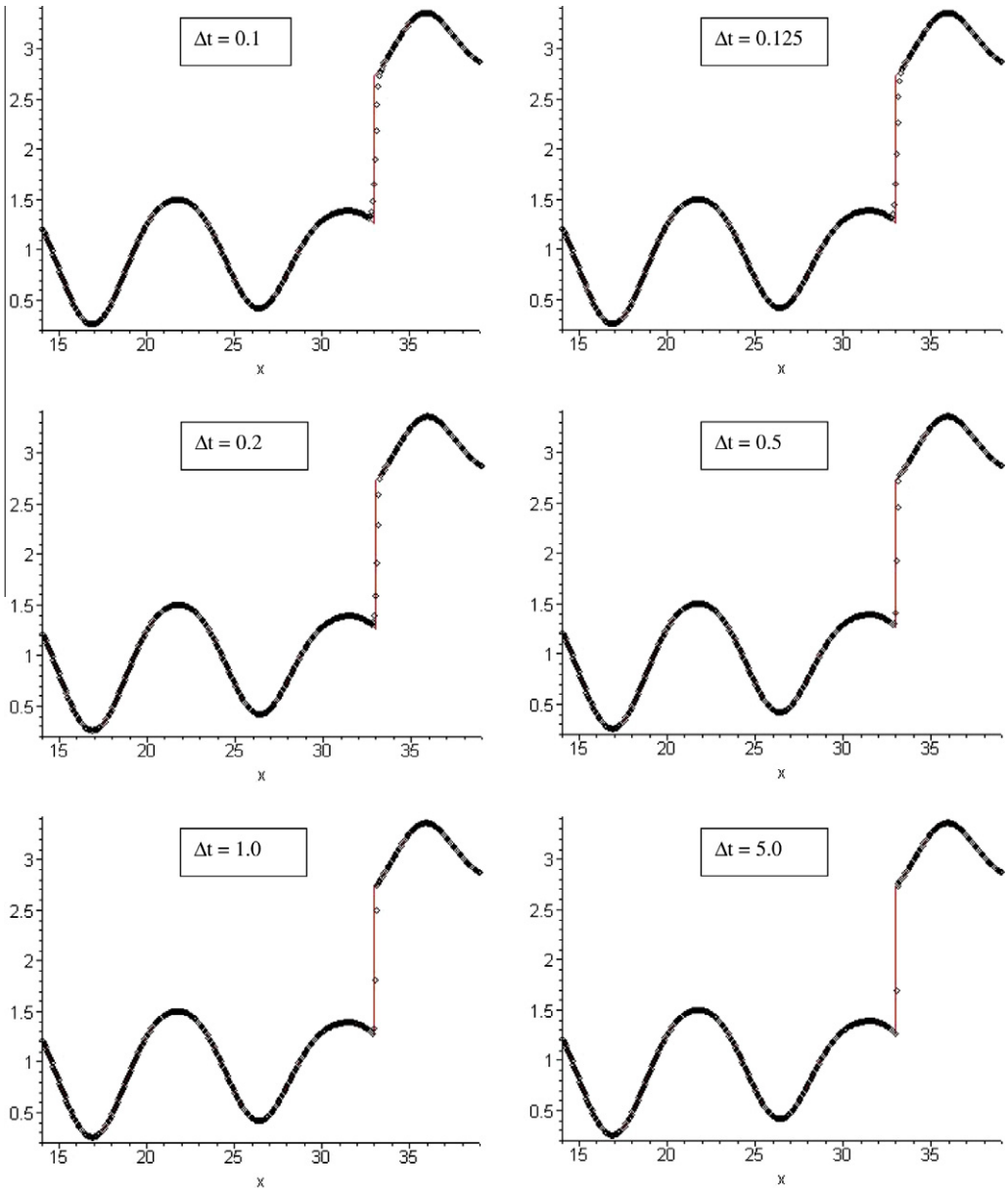

Fig. 7. Exact (–) and numerical (○) solutions of Example 2 at $t_f = 5$ for different values of Δt.

6.4. Example 4: Compressible flow

In this case, we simulate the transport of a concentration-hill (with corners) by compressible flow. We consider Eq. (80) with $v = x - 0.5$. The computation was performed in the domain $0 \leqslant x \leqslant 1$. As initial data we take the hill of the form

$$C(x,0) = 0.25[1 + \cos(\pi\lambda x)], \tag{88}$$

where

$$\lambda = \min(|x - 0.5|; 0.2)/0.2. \tag{89}$$

As shown in Fig. 9, the solutions computed by PT method, at $t_f = 0.25$, are in agreement with the exact solutions (even in the corners), for several values of Δt. In this example, we observe that $(N_{Co})_{max} = 0.25$, if $\Delta t = 0.00125$, and $(N_{Co})_{max} = 50$, if $\Delta t = t_f = 0.25$, where

$$(N_{Co})_{max} \equiv \frac{\Delta t}{\Delta x} \max_{0 \leqslant x \leqslant 1} |v(x)|. \tag{90}$$

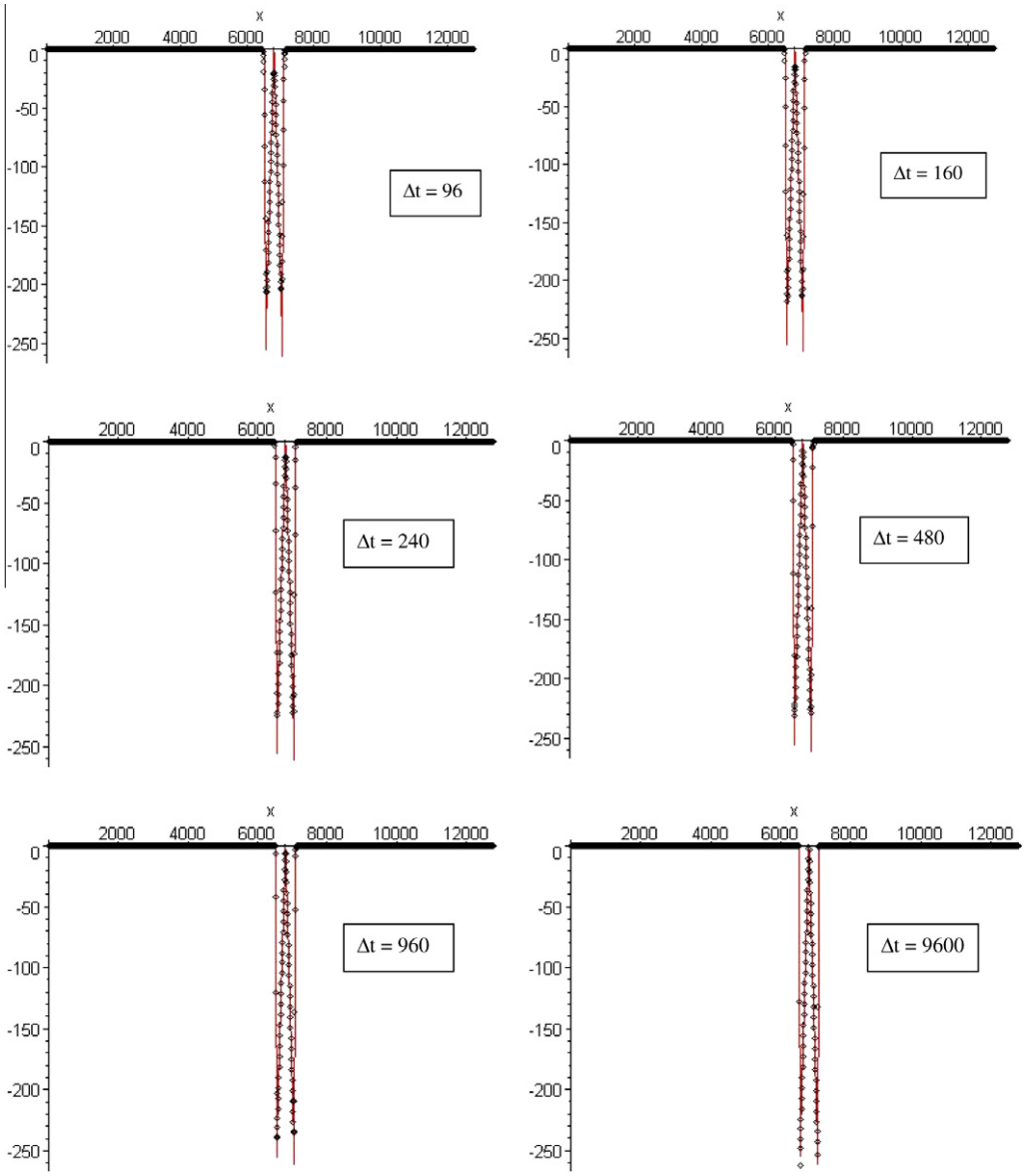

Fig. 8. Exact (–) and numerical (○) solutions of Example 3 at $t_f = 9600$ for different values of Δt.

7. Numerical examples in two dimensions

7.1. Example 5: Rotation of a circular cone

Solid body rotation is a classical test for advection algorithms. Generally, it is considered a domain $B = [0,L_x] \times [0,L_y]$ and a function $f : B \subset \mathbb{R}^2 \to \mathbb{R}$, whose the graph defines the position of a three-dimensional body at some initial instant. The body is rotated (counterclockwise) with angular velocity ω, around a fixed axis that passes through the point $(x_0,y_0) \in B$ and has direction normal to the xy-plane. Hence, the values that represent the velocities in the x and y directions are

$$u = -\omega(y - y_0), \tag{91}$$

$$v = \omega(x - x_0). \tag{92}$$

The partial differential equation that describe this movement is the following advection equation

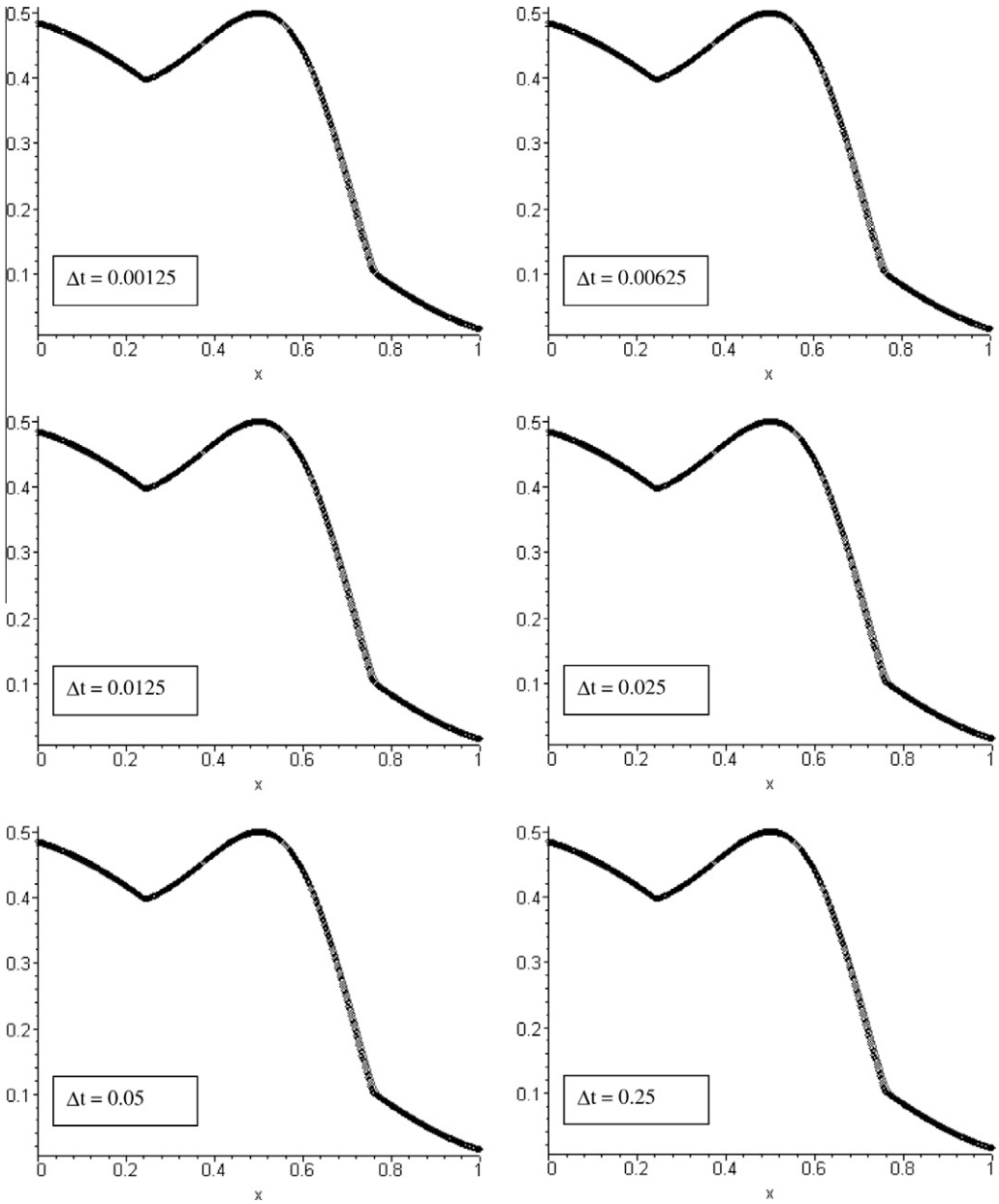

Fig. 9. Exact (–) and numerical (∘) solutions of Example 4 at $t_f = 0.25$ for different values of Δt.

$$\frac{\partial C}{\partial t}+\frac{\partial (uC)}{\partial x}+\frac{\partial (vC)}{\partial y}=0, \tag{93}$$

with initial condition given by

$$C(x,y,0)=f(x,y). \tag{94}$$

We consider the rotation of a circular cone, where $B=[0,2\ ]\times[0,2]$, $x_0=y_0=1,\omega=1$ and

$$f(x,y)=\begin{cases}\sqrt{3}\left[r-\sqrt{(x-x_c)^2+(y-y_c)^2}\right], & \text{if } (x-x_c)^2+(y-y_c)^2\leqslant r^2\\ 0, & \text{otherwise}\end{cases}, \tag{95}$$

with $x_c=1$, $y_c=1.25$ and $r=0.70$.

In this example, the path lines are evaluated analytically.

The plots in Fig. 10 show the numerical and exact solutions after two evolutions, with $\Delta t=4\pi$ and $\Delta x=\Delta y=0.005$.

Here, in addition, the accuracy of PT method is measured using the numerical error ε_2, given by

$$\varepsilon_2=\sqrt{\frac{\sum_{i,j}\left(C_{i,j}^{\text{numer.}}-C_{i,j}^{\text{theor.}}\right)^2}{\sum_{i,j}\left(C_{i,j}^{\text{theor.}}\right)^2}}. \tag{96}$$

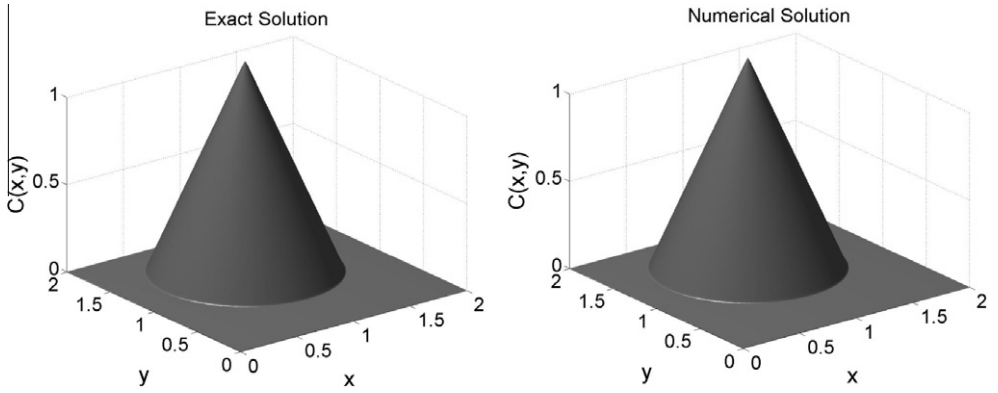

Fig. 10. Exact and numerical solutions of Example 5.

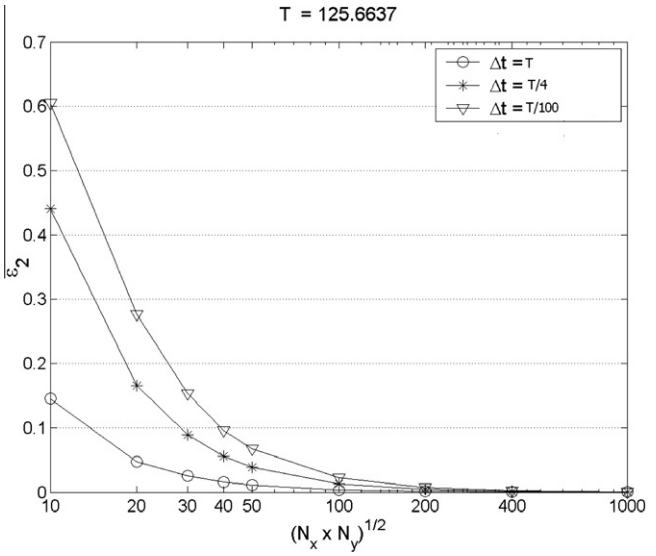

Fig. 11. The error ε_2 after twenty complete evolutions of the circular cone, with three different values of Δt.

Fig. 11 shows the error ε_2 after twenty complete evolutions of the circular cone for three values of Δt, where N_x and N_y are the block numbers in the directions x and y, respectively. We note that, for a given grid, the error increases as the time step decreases, and vice versa. Besides, $\varepsilon_2 \to 0$, whenever $\Delta x, \Delta y \to 0$.

7.2. Example 6: Deformation of a cylinder

Following Leveque [19], we consider the swirling deformation flow:

$$u(x,y,t) = \sin^2(\pi x)\sin(2\pi y)g(t), \tag{97}$$

$$v(x,y,t) = -\sin^2(\pi y)\sin(2\pi x)g(t). \tag{98}$$

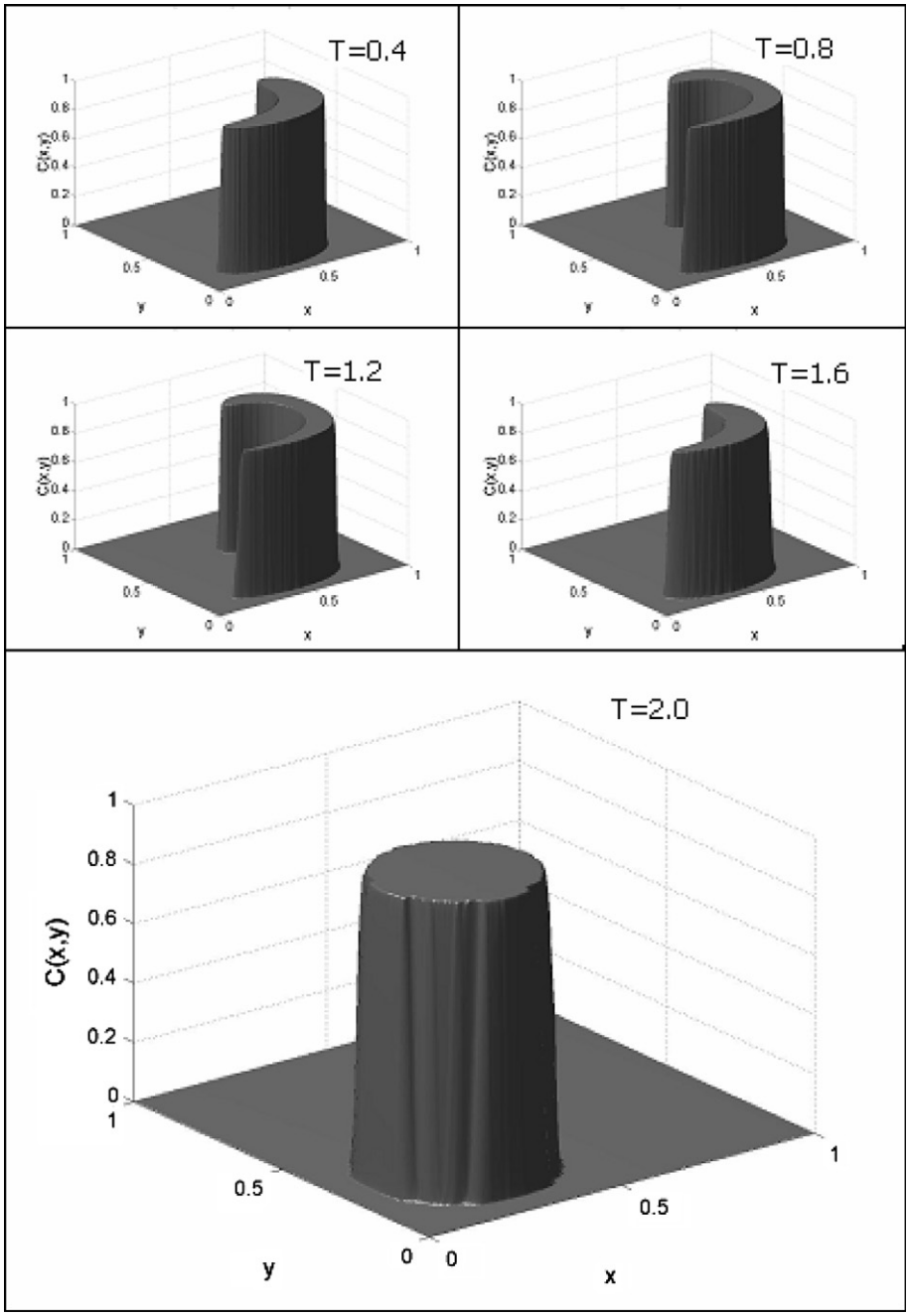

Fig. 12. Five stages of the swirling deformation flow.

This flow is defined on the domain $B = [0,1] \times [0,1]$. The function $g(t) = \cos(\pi t/t_f)$ is used to introduce time dependence on the interval $0 \leqslant t \leqslant t_f$. This flow field reverses direction at the instant that $t = t_f/2$ (instant of larger deformation) in such a way that the initial condition is recovered at final time t_f, i.e., $C(x,y,t_f) = C(x,y,0)$.

Here we use $t_f = 2$. The initial condition for the differential equation described in Eq. (93) is (essentially) a cylinder, given by

$$C(x,y,0) = \begin{cases} 1, & \text{if } (x-0.3)^2 + (y-0.3)^2 \leqslant (0.2)^2 \\ 0, & \text{otherwise} \end{cases} \tag{99}$$

We consider $\Delta x = \Delta y = 0.02$ and $\Delta t = 0.4$. Note that this spatial grid is relatively coarse. In fact, in Example 7.1 we use $\Delta x = \Delta y = 0.005$.

In the backtracking step, given $\mathbf{v} = (u,v)$ we solve the system of differential equations $d\mathbf{x}/dt = \mathbf{v}$, subject to final conditions $x(t+\Delta t) = \tilde{x}$ and $y(t+\Delta t) = \tilde{y}$, using an appropriate backward algorithm. Such algorithm combines n steps of the classical Runge–Kutta method of order 4 with $m-n$ steps of an implicit method, also of order 4, see [20]. This backward algorithm is described below, where we consider $m = 80$ and $n = 3$. Since $\Delta t = 0.4$, in this case we have $h \equiv \Delta\, t/m = 0.005$.

Backward Algorithm

Data. $t,\ \Delta t,\ \tilde{x} = x(t+\Delta t),\ \tilde{y} = y(t+\Delta t),\ m \geqslant 3,$ and $3 \leqslant n \leqslant m$.

Step 1. Set $h = \Delta t/m$ and $t_m = t + \Delta t$.
Step 2. Set $x^{(m)} = \tilde{x}, y^{(m)} = \tilde{y}$, and $\mathbf{x}^{(m)} = (x^{(m)}, y^{(m)})$.
Step 3. For $j = m$ util $m-(n-1)$, set:

$$\mathbf{k}_1^{(j)} = \mathbf{v}\left(x^{(j)}, y^{(j)}, t_j\right) \equiv \left(k_{11}^{(j)}, k_{12}^{(j)}\right),$$

$$\mathbf{k}_2^{(j)} = \mathbf{v}\left(x^{(j)} - \frac{h}{2}k_{11}^{(j)}, y^{(j)} - \frac{h}{2}k_{12}^{(j)}, t_j - \frac{h}{2}\right) \equiv \left(k_{21}^{(j)}, k_{22}^{(j)}\right),$$

$$\mathbf{k}_3^{(j)} = \mathbf{v}\left(x^{(j)} - \frac{h}{2}k_{21}^{(j)}, y^{(j)} - \frac{h}{2}k_{22}^{(j)}, t_j - \frac{h}{2}\right) \equiv \left(k_{31}^{(j)}, k_{32}^{(j)}\right),$$

$$\mathbf{k}_4^{(j)} = \mathbf{v}\left(x^{(j)} - hk_{31}^{(j)}, y^{(j)} - hk_{32}^{(j)}, t_j - h\right) \equiv \left(k_{41}^{(j)}, k_{42}^{(j)}\right),$$

$$\mathbf{x}^{(j-1)} = \mathbf{x}^{(j)} - \frac{h}{6}\left(\mathbf{k}_1^{(j)} + 2\mathbf{k}_2^{(j)} + 2\mathbf{k}_3^{(j)} + \mathbf{k}_4^{(j)}\right) \equiv \left(x^{(j-1)}, y^{(j-1)}\right),$$

$$t_{j-1} = t_j - h.$$

Step 4. For $j = m-n$ util 1, To obtain $x^{(j-1)}$ and $y^{(j-1)}$, solve the following nonlinear system:

$$\begin{cases} x^{(j-1)} = \frac{1}{25}\left[x^{(j)} - 36x^{(j+1)} + 16x^{(j+2)} - 3x^{(j+3)} - 12hu(x^{(j-1)}, y^{(j-1)}, t^{(j-1)})\right] \\ y^{(j-1)} = \frac{1}{25}\left[y^{(j)} - 36y^{(j+1)} + 16y^{(j+2)} - 3y^{(j+3)} - 12hv(x^{(j-1)}, y^{(j-1)}, t^{(j-1)})\right] \end{cases}$$

Set $\mathbf{x}^{(j-1)} = (x^{(j-1)}, y^{(j-1)})$

Set $t_{j-1} = t_j - h$.

Five steps of this flow obtained by the present methodology are shown in Fig. 12. The numerical solutions show that the flow indeed reverses directions. Besides, at final time $t = 2$, the path tubes method is capable to recover (approximately) the initial condition indicated in Eq. (99).

8. Conclusion

We have proposed new approaches for the path tubes (PT) method, a semi-Lagrangian metodology for advection equations that was presented in a recent article by Henderson et al. [4].

Summarizing, in this work, the following objectives have been achieved: (a) it was developed a 1D integral formulation for PT method, (b) this formulation led to an accurate discretization scheme for one-dimentional advection equations, which uses the three-point Gauss quadrature rule and a modified cubic Lagrangian interpolation with flux limiters, (c) using the change of variable formula and the trapezoidal rule, it was deduced a new and attractive multidimensional discretization scheme, which works also with a modified multidimensional cubic Lagrangian interpolation with flux limiters, (d) considering an 1D scheme, it was shown that PT method is unconditionally stable, (e) using both 1D and 2D problems, the new schemes were tested on a classical numerical benchmark with difficult examples.

We would like to emphasize that PT method is an explicit scheme, which is not subject to CFL condition. Thus, different from many conventional schemes, PT method can work with time steps that are considered as of great magnitude. Besides, PT scheme is a (locally) conservative formulation, whose behavior of the generated solution is non-oscillatory and non-diffusive.

In spite of none three-dimensional problem to have been solved here, it should be observed that the application of the multidimensional scheme shown in Section 5.2 to 3D problems is an immediate consequence. Such applications will be considered in our future works.

Acknowledgements

The research by N. Henderson has been carried out in the framework of project PROCIENCIA-UERJ financed by FAPERJ. Partial support for this work was also provided to M. Sampaio by FAPERJ. N. Henderson gratefully acknowledges the research grant provided by CNPq (Conselho Nacional de Desenvolvimento Científico e Tecnológico, Ministry of Science & Technology, Brazil).

References

[1] R.J. Leveque, Finite volume methods for hyperbolic problems, Cambridge Texts in Applied Mathematics, Cambridge University Press, 2002.
[2] J.W. Thomas, Numerical partial differential equations: finite difference methods, Texts in Applied Mathematics, vol. 22, Springer, New York, 1995.
[3] J.W. Thomas, Numerical partial differential equations: conservation laws and elliptic equations, Texts in Applied Mathematics, vol. 33, Springer, New York, 1999.
[4] N. Henderson, M. Sampaio, L. Pena, Path tubes method: a semi-Lagrangian approach for linear advection equations, Chem. Eng. Sci. 64 (2009) 3138.
[5] A. Wiin-Nielsen, On the applications of trajectory methods in numerical forecasting, Tellus 11 (1959) 180.
[6] J.G. Trulio, Report AFWL-TR-66-19, Air Force Weapons Laboratory, Kirtland Air Force, USA, 1965.
[7] C.W. Hirt, J.L. Cook, T.D. Butler, A Lagrangian method for calculation the dynamics of an incompressible fluid with free surface, J. Comput. Phys. 5 (1970) 103.
[8] A. Robert, A semi-Lagrangian semi-implicit numerical integration scheme for the primitive meteorological equations, J. Meteorolog. Soc. Jpn. 60 (1982) 319.
[9] A. Staniforth, J. Côté, Semi-Lagrangian integration schemes for atmospheric models – a review, Monthly Weather Rev. 119 (1991) 2206.
[10] P.K. Smolarkiewicz, J.A. Pudykiewicz, A class of semi-Lagrangian approximations for fluids, J. Atmos. Sci. 49 (1992) 2082.
[11] D.L. Williamson, J.G. Olson, A comparison of semi-Lagrangian and Eulerian polar climate simulation, Monthly Weather Rev. 126 (1998) 991.
[12] S. Gravel, A. Staniforth, A mass conservative semi-Lagrangian scheme for the shallow wave equation, Monthly Weather Rev. 122 (1994) 243.
[13] A. Chilakapati, A characteristic-conservative model for Darcian advection, Adv. Water Resour. 22 (1999) 597.
[14] M.E. Gurtin, An Introduction to Continuun Mechanics, Academic Press, New York, 1981.
[15] C. Truesdell, R.A. Toupin, Classical field theories of mechanics, Handbuch der Physik III/1, Springer, Berlin, 1960.
[16] R.G. Bartle, The Elements of Real Analysis, secon ed., Wiley, New York, 1976.
[17] M. Abramowitz, I.M. Stegun, Handbook of Mathematical Functions, Dover, New York, 1970.
[18] J. Stoer, R. Bulirsch, Introduction to Numerical Analysis, Springer-Verlag, New York, 1980.
[19] R.J. Leveque, High-resolution conservative algorithms for advection in incompressible flow, SIAM J. Numer. Anal. 33 (1996) 627.
[20] W.E. Boyce, R.C. DiPrima, Elementary Differential Equations and Boundary Value Problems, eighth ed., John Wiley, New York, 2005.